scientific reports

Check for updates

OPEN

Detection of quadratic phase coupling by cross-bicoherence and spectral Granger causality in bifrequencies interactions

Takeshi Abe[1,5,6], Yoshiyuki Asai[1,2,5], Alessandra Lintas[3,4] & Alessandro E. P. Villa[4,6]

Quadratic Phase Coupling (QPC) serves as an essential statistical instrument for evaluating nonlinear synchronization within multivariate time series data, especially in signal processing and neuroscience fields. This study explores the precision of QPC detection using numerical estimates derived from cross-bicoherence and bivariate Granger causality within a straightforward, yet noisy, instantaneous multiplier model. It further assesses the impact of accidental statistically significant bifrequency interactions, introducing new metrics such as the ratio of bispectral quadratic phase coupling and the ratio of bivariate Granger causality quadratic phase coupling. Ratios nearing 1 signify a high degree of accuracy in detecting QPC. The coupling strength between interacting channels is identified as a key element that introduces nonlinearities, influencing the signal-to-noise ratio in the output channel. The model is tested across 59 experimental conditions of simulated recordings, with each condition evaluated against six coupling strength values, covering a wide range of carrier frequencies to examine a broad spectrum of scenarios. The findings demonstrate that the bispectral method outperforms bivariate Granger causality, particularly in identifying specific QPC under conditions of very weak couplings and in the presence of noise. The detection of specific QPC is crucial for neuroscience applications aimed at better understanding the temporal and spatial coordination between different brain regions.

Abbreviations

GC	Granger causality
QPC	Quadratic phase coupling
R_{BQPC}	Ratio of bispectral quadratic phase coupling
R_{GQPC}	Ratio of bivariate Granger causality quadratic phase coupling

The detection of nonlinear interrelations in multivariate time series is a crucial challenge in analyzing complex systems across diverse fields, including neuroscience, environmental science, economics, and engineering. Nonlinear signals can be characterized by higher-order statistics in both the time domain (such as higher-order cumulants) and the frequency domain (such as the Fourier transform of higher-order cumulants, leading to higher-order spectra)[1–4]. The inherent complexity of nonlinear dynamics means that interactions can be subtle, often obscured by noise or non-stationary signals. This subtlety requires careful methodological consideration to accurately distinguish causality from mere correlation in observed interrelations, thereby avoiding erroneous conclusions about the system's underlying dynamics.

[1]AI Systems Medicine Research and Training Center, Graduate School of Medicine and University Hospital, Yamaguchi University, Yamaguchi 755-8505, Japan. [2]Department of Systems Bioinformatics, Graduate School of Medicine, Yamaguchi University, Yamaguchi 755-8505, Japan. [3]HEC-LABEX, University of Lausanne, Quartier UNIL-Chamberonne, 1015 Lausanne, Switzerland. [4]Neuroheuristic Research Group & Complexity Sciences Research Group, University of Lausanne, Quartier UNIL-Chamberonne, 1015 Lausanne, Switzerland. [5]Division of Systems Medicine and Informatics, Research Institute of Cell Design Medical Science, Yamaguchi University, Yamaguchi 755-8505, Japan. [6]These authors contributed equally: Takeshi Abe and Alessandro E. P. Villa. ✉email: alessandro.villa@unil.ch

The analysis of time series by wavelet transforms provides insights into both time and frequency domains simultaneously[5–8]. This dual perspective is crucial for detecting nonlinear interactions that may vary over time. Alternatively, information-theoretic approaches quantify the flow of information between variables, capturing nonlinear dependencies through concepts such as mutual information, transfer entropy, and symbolic dynamics. Among these, mutual information (MI), especially when combined with Fourier transform surrogates, is particularly effective at distinguishing between linear and nonlinear interrelations and at detecting various forms of nonlinear interactions[9]. These interactions, potentially occurring at any order, offer insights into the underlying dynamics and interactions of systems—insights that are not accessible through linear analysis alone—including, but not limited to, phase synchronization, amplitude modulation, and more complex dynamics such as quadratic or higher-order phase coupling.

Phase coupling is a phenomenon where the phase (timing) of oscillations in one signal becomes correlated with the phase of oscillations in another signal. This implies that the two signals are not only correlated in their amplitudes but also in their timing. Quadratic Phase Coupling (QPC) goes a step further by capturing higher-order phase relationships between signals. It quantifies how the product of the instantaneous phases of two signals is related, indicating nonlinear phase interactions. The presence of QPC in a system, especially when compared to the detection of general nonlinearities is particularly noteworthy to detect the synchronization of biological rhythms or the modulation of signals in electronic and optical systems[10–12]. This is especially useful in fields like neuroscience, where understanding the phase relationships between neuronal signals detected by QPC might correlate with certain cognitive states, pathological conditions, or responses to stimuli and functional brain connectivity[13–20].

Cross-bicoherence is a statistical measure used to assess phase coupling or nonlinear interactions between different frequency components in multivariate time series data. It is an extension of the bicoherence, which is a measure of the second-order spectral density of a signal. Cross-bicoherence specifically quantifies the degree to which the phases of two different signals at distinct frequencies are nonlinearly coupled or synchronized[21–23]. Establishing significance thresholds is essential for making reliable inferences about phase coupling in experimental data, particularly in applications such as neuroscience, where understanding brain connectivity and synchronization is of paramount importance. Several approaches have been carried out to develop statistical tests. Analytical methods assume specific statistical distributions for the cross-bicoherence values under the null hypothesis that its ground-truth value is zero[24,25]. Computational approaches include bootstrap resampling and permutation methods generating a large number of resampled datasets from the original data[26] and Monte Carlo simulations generating surrogate data that mimic the statistical properties of the experimental data to create a null distribution[27]. By comparing the observed cross-bicoherence with the null distribution, statistical significance can be determined.

An alternative way to detect QPC is represented by bivariate Granger causality. The traditional Granger causality (GC) test is used to quantitative measuring whether one time series can predict another time series and to assess the magnitude of causal effects[28,29]. It can identify the direction of causality, thus determining which of the two time series leads in terms of causality[30]. Furthermore, GC goes beyond linear relationships, enabling the detection of nonlinear interactions between time series variables[31]. However, the conventional pairwise method for analyzing GC may not effectively differentiate between direct causal influences originating from one time series and indirect influences that operate through a third time series. This problem has been overcome by deriving a conditional GC in the frequency domain[32–34]. Such bivariate GC specifically determines the causal influence between two variables while accounting for the potential influence of other variables[35]. The corresponding statistics evaluation of significance include parametric tests[36,37], nonparametric tests[38] and various bootstrap testing approaches[34,39]. Nevertheless, estimation bias resulting from perturbations in observed time series data may generate potentially misleading statistically significant values, thus challenging true evidence of QPC even when considering the theoretical null distribution of the statistics.

The objective of this study is to identify specific QPC produced by the carrying frequencies of interacting channels within a basic, noisy instantaneous multiplier model. Our analysis revolves around examining the impact of a pair of interacting time series exhibiting varying degrees of coupling strength to a third time series. These time series represent stationary stochastic processes simulating experimental brain signals driven by independent oscillatory inputs, along with added noise. Our primary contribution lies in establishing a computational framework for the assessment of QPC detection. We utilize two analytical techniques: cross-bicoherence analysis and bivariate Granger causality. In both cases, we introduce an empirical Bayes method for the significance testing of the null hypothesis, specifically focusing on assessing whether the statistics are zero at given pairs of frequencies, known as bifrequencies. To evaluate the accuracy of QPC detection, we employ a false discovery rate inference methodology. This approach involves comparing the bifrequencies associated with significant statistics derived from the experimental time series to those expected from the phase coupling of the interacting channels' carrying frequencies. Our findings indicate that the detection of specific QPC by cross-bicoherence analysis outperforms that by bivariate Granger causality, particularly in the presence of noise and when dealing with weak coupling among the interacting channels. We also discuss the potential applications of our results in the context of characterizing interaction networks, especially in the field of neuroscience.

Results

A three-channel model of bifrequencies interaction

We consider a simple model with three distinct channels labeled X_1, X_2, and X_3. Each channel receives input signals that are periodic, each one with its unique frequency denoted as F_i (measured in Hz). The input signals are represented by three functions $I_1(t, \nu)$ (a triangular wave), $I_2(t, \nu)$ (a rectangular wave), and $I_3(t, \nu)$ (a cosine wave) as a function of continuous time t ($t \in \mathbb{R}$) and a sample index ν. The use of triangular and rectangular

waveforms is meant to endow our model with two advantageous properties. Firstly, the power distribution of these waveforms is more varied than that of pure sinusoids, thus being more closely mimicking the power-law spectrum commonly observed in nature. Secondly, the expected signal-to-noise ratio for each channel can be derived analytically (as detailed in the "Supplementary Material"), allowing for a more detailed analysis of the model's performance in different conditions.

For each sample ν, the initial phase parameter $\omega_i = \omega_i(\nu)$ of each signal I_i is given a random shift. This shift follows a uniform distribution over the interval $[0, 2\pi)$, meaning the initial phase parameter can be any value between 0 and just under 2π radians, with all values within this range being equally probable. The periodic functions I_i are defined as follows:

$$I_1(t, \nu) = 2 \operatorname{asin}(\sin(2\pi F_1 t + \omega_1(\nu))); \tag{1}$$

$$I_2(t, \nu) = \begin{cases} 1 & 0 \leq (2\pi F_2 t + \omega_2(\nu)) \bmod 2\pi < \pi; \\ -1 & \text{otherwise} \end{cases} \tag{2}$$

$$I_3(t, \nu) = \cos(2\pi F_3 t + \omega_3(\nu)). \tag{3}$$

An independent white noise is added to each channel (ξ_1, ξ_2, ξ_3), following a standard Gaussian distribution (mean $\mu = 0$, standard deviation $\sigma = 1$). In addition, channel X_3 receives an input from interacting channels X_1 and X_2 depending on a coupling strength $W_{(1,2)}$ (Fig. 1). The following equations define the three-channel model as a set of stochastic processes:

$$X_1(t, \nu) = I_1(t, \nu) + \xi_1(t, \nu); \tag{4}$$

$$X_2(t, \nu) = I_2(t, \nu) + \xi_2(t, \nu); \tag{5}$$

$$X_3(t, \nu) = W_{(1,2)} X_1(t, \nu) X_2(t, \nu) + I_3(t, \nu) + \xi_3(t, \nu). \tag{6}$$

The detection of specific QPC was tested for distinct bifrequencies (F_1, F_2) of channels X_1 and X_2 in the set of values $[(70/2\pi), (80/2\pi), (120/2\pi), (150/2\pi), (230/2\pi), (50 - 10/2\pi)]$. We divided the parameter value of the frequency by constant 2π in order to cancel out the 2π in the argument of the trigonometric function in Eqs. (1–3). The carrying frequency F_3 of channel X_3 was chosen in the same set of frequency values, but distinct from F_1, F_2, and $F_1 + F_2$. The coupling strengths $W_{(1,2)}$ were chosen in the set $[0.025, 0.050, 0.075, 0.150, 0.300, 0.750]$, ranging from weak to strong. Three time series of 64000 points were generated for an experimental condition defined by each set of parameters.

Each time series was created by merging 128 independent epochs, with each epoch corresponding to a 5-second interval sampled at 100 Hz. Each epoch contained an independent input signal phase parameters and white noise. Four 5-second epochs of the three-dimensional time series (X_1, X_2, X_3) are depicted in Fig. 2. It should be noted that the X_1 and X_2 time series are identical in panels Fig. 2A and C, as well as in panels Fig. 2B and D. The differences observed in the respective X_3 time series are solely attributed to a different coupling strength, $W_{(1,2)}$, between the interacting signals X_1 and X_2. Interestingly, a strong coupling strength leads to an overall
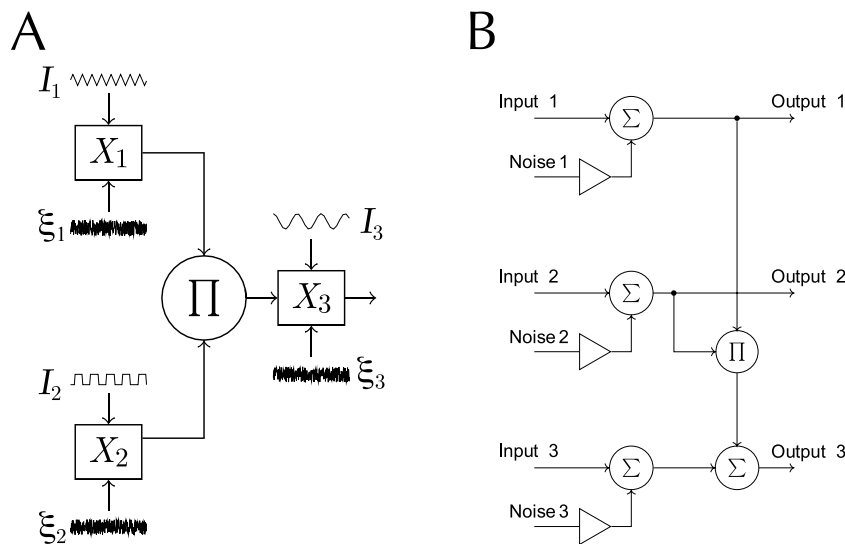
Figure 1. A three-channel model of bifrequencies interaction. (**A**) Schematic diagram of the model with input signal I_i, noise ξ_i, and output X_i corresponding to channel i. (**B**) The corresponding block diagram.
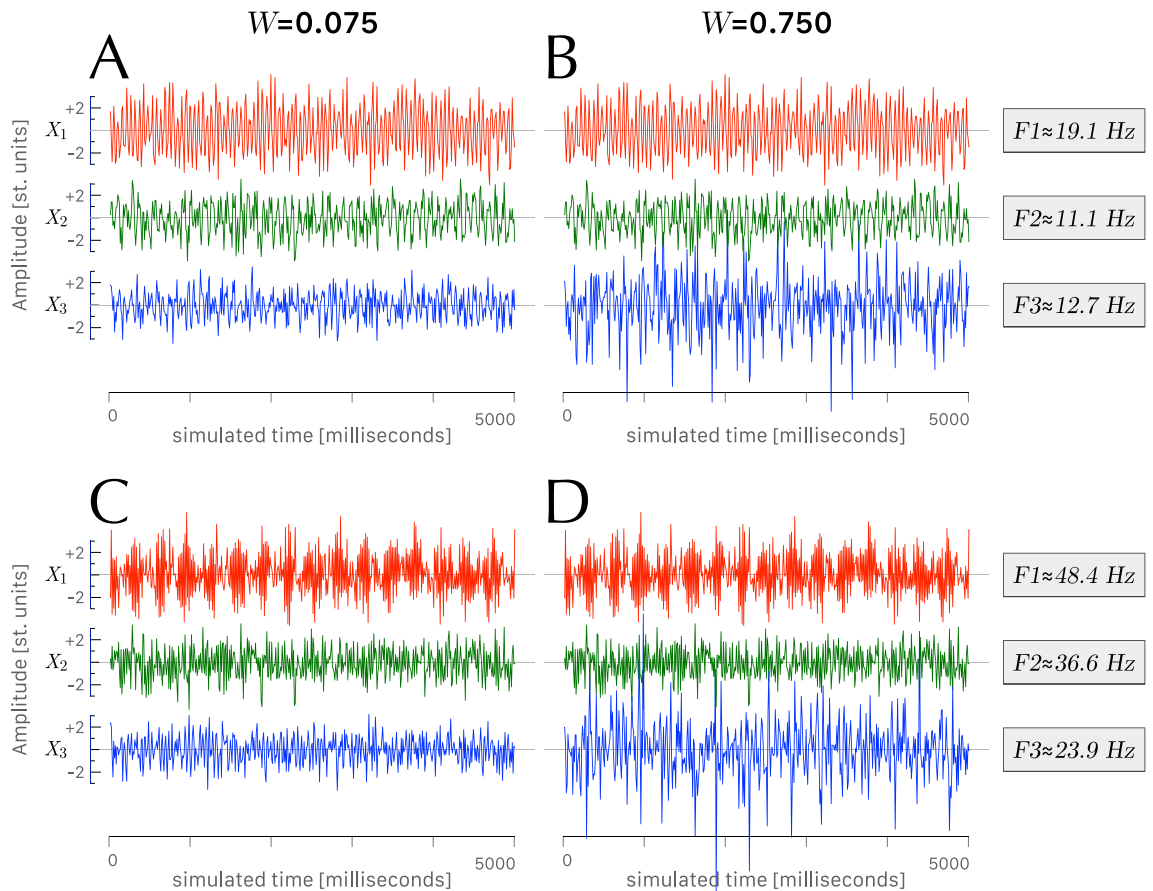
Figure 2. Four 5-second epochs of the three dimensional time series (X_1, X_2, X_3) for small coupling $W_{(1,2)}$ (panels **A**, **C**) and large coupling $W_{(1,2)}$ (panels **B**, **D**). (**A**, **B**) Experimental condition with carrying frequencies $F_1 = (120/2\pi) \approx 19.1$ Hz, $F_2 = (70/2\pi) \approx 11.1$ Hz, and $F_3 = (80/2\pi) \approx 12.7$ Hz. (**C**, **D**) Experimental condition with carrying frequencies $F_1 = (50 - 10/2\pi) \approx 48.4$ Hz, $F_2 = (230/2\pi) \approx 36.6$ Hz, and $F_3 = (150/2\pi) \approx 23.9$ Hz.

amplification of the output signal X_3 in a nonlinear way, along with a predominant presence of frequency F_3 carried by channel 3. In total, 354 experimental conditions were examined (59 conditions for each value of coupling strength). For each condition we computed the R_{BQPC} (i.e., the ratio of bispectral quadratic phase coupling) and the R_{GQPC} (i.e., the ratio of bivariate Granger causality quadratic phase coupling).

Quadratic phase coupling computed by cross-bicoherence and by Granger causality

We investigated how cross-bicoherence and bivariate GC were comparable in detecting quadratic phase coupling in two sectors of the cross-bicoherence domain for various coupling strengths(Fig. 3). Figure 3A,B illustrates the detection of QPC in sector Q_I with $F_1 = (120/2\pi)$, $F_2 = (70/2\pi)$, and $F_3 = (80/2\pi)$, and Fig. 3C,D illustrates the detection of QPC in sector Q_{II} with $F_1 = (50 - 10/2\pi)$, $F_2 = (230/2\pi)$, and $F_3 = (150/2\pi)$. Both methods show an increase in spurious values that affect the detection of specific QPC. In cross-bicoherence significance maps, these spurious values are represented by an increase in black bins along the axis corresponding to carrier frequencies F_1 and F_2, with an increase in coupling strength between the interacting channels X_1 and X_2 (Fig. 3A,C). In median unconditional bivariate GC spectrum, these spurious values are represented by an increase in overall significant causal dependency values and more specifically by a shift of the peak in this curve towards the value of the carrier frequency F_3 of channel X_3, represented by the blue labels and blue arrows (Fig. 3B,D).

Building upon the preceding findings, the subsequent comparison of the specific QPC detection methods involves a two-way analysis of variance. This analysis incorporates the ratio of specific QPC as dependent variable, with three primary factors under consideration: method (consisting of 2 levels, "bispectral" and "bivariate GC"), coupling strength (comprising 5 levels, namely [0.025, 0.050, 0.075, 0.150, 0.300, 0.750]) and sector Q (consisting of 2 levels, Q_I and Q_{II}). In this analysis, we have omitted the outlier values of the dependent variables, specifically, those with specific QPC ratios equal to zero or equal to 1. Both distributions of the indices show significant difference between variances across factor levels (Levene's test $F(11, 292) = 6.62$, $p < .001$ and $F(11, 229) = 4.20$, $p < .001$ for R_{BQPC} and R_{GQPC}, respectively). Therefore, the homogeneity of variances in the different factor levels cannot be assumed. The assumption of normality of the QPC ratios is not supported
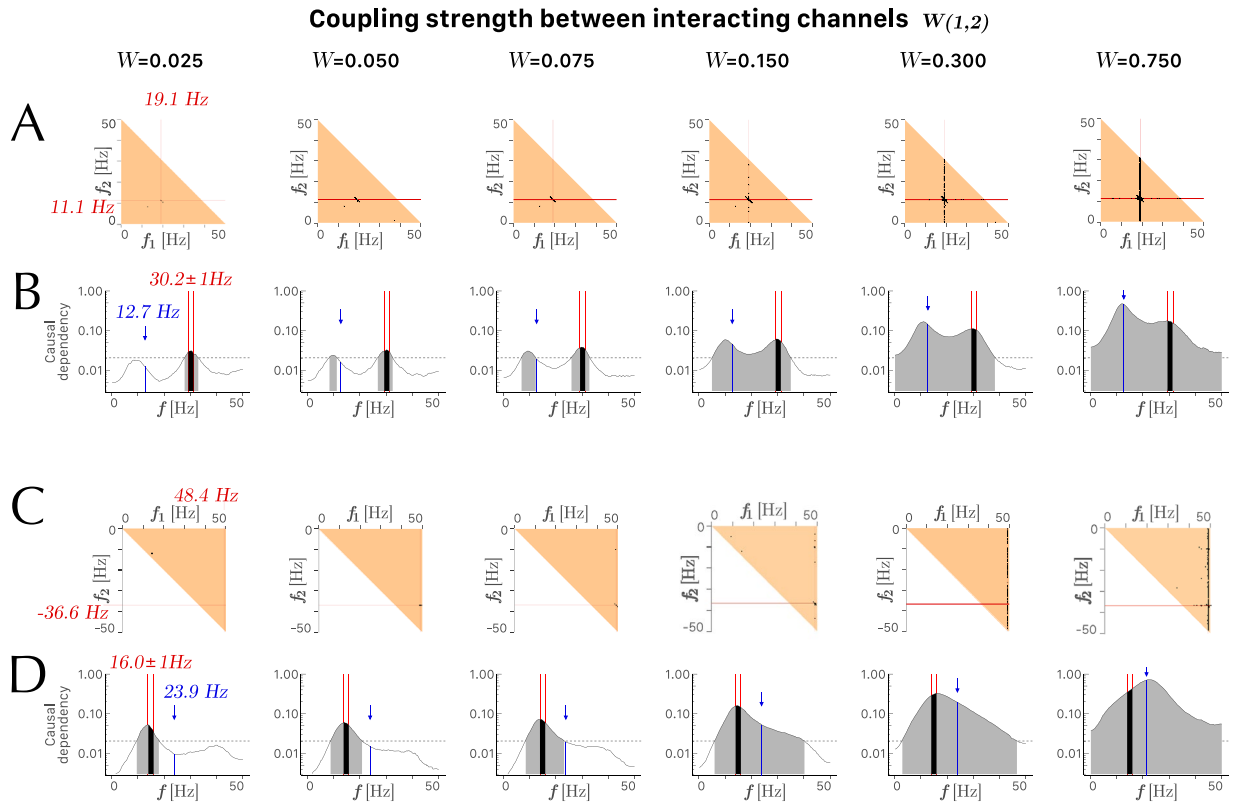
Figure 3. Examples of a three-channel model of bifrequencies interaction (Fig. 1) from channels (X_1, X_2) to channel X_3 in the 0–50 Hz range with cross-channel coupling strength varying from weak to strong (from left to right). Panels in rows (**A**) and (**C**) show the cross-bicoherence significance maps with only those bifrequencies (black bins) characterized by cross-bicoherence values different from zero ($\overline{b_{ijk}^2}, q < .05$). Panels in rows (**B**) and (**D**) show the median unconditional bivariate Granger causality spectrum in a semi-logarithmic scale with a grey area corresponding to the integration over the curve of all significant values (with a threshold of significance represented by the dashed line) and a black area corresponding to the integration for the spectral interval of interest. (**A**, **B**) Analyses falling in sector Q_I at bifrequencies $F_1 = (120/2\pi), F_2 = (70/2\pi)$ indicated by the red labels and $F_3 = (80/2\pi)$ indicated by the blue label and arrow (i.e., $F_1 \approx 19.1$ Hz, $F_2 \approx 11.1$ Hz, $F_3 \approx 12.7$ Hz). (**C**, **D**) Analyses falling in sector Q_{II} at bifrequencies $F_1 = (50 - 10/2\pi), F_2 = (230/2\pi)$ indicated by the red labels and $F_3 = (150/2\pi)$ indicated by the blue label and arrow (i.e., $F_1 \approx 48.4$ Hz, $F_2 \approx 36.6$ Hz, $F_3 \approx 23.9$ Hz). In the plots, f_1 and f_2 correspond to the bifrequency coordinates of frequency parameters (F_1, F_2).

by the Shapiro-Wilk test ($p < .001$ for both R_{BQPC} and R_{GQPC}). Then, our data did not meet the assumptions of the parametric ANOVA. As an alternative we run a three-way ANOVA on the ranks of QPC ratios. The method and the coupling strength $W_{(1,2)}$ are very significant factor variables ($F(1, 521) = 37.249, p < .001$ and $F(5, 521) = 44.753, p < .001$, respectively) as illustrated by Fig. 4 for both methods. The values of R_{BQPC} were larger than R_{GQPC} at any tested values of coupling strength (Wilcoxon tests, always $p < .001$ with a large effect size). Notice that the curve of R_{BQPC} is non-monotonic (Fig. 4A) with a median peak value of 0.497 occurring with $W_{(1,2)} = 0.050$, whereas the curve of R_{BGPC} is monotonically decreasing (Fig. 4B) with a median peak value of 0.119 at $W_{(1,2)} = 0.025$. It is also worth noting that in the three-way ANOVA the main factor sector Q is not significant ($F(1, 521) = 1.906, p = .168$).

Effect of coupling strength between interacting channels on signal-to-noise ratio

The signal-to-noise ratio (SNR) for any non-zero frequency of the input periodic signals X_i, is computed as

$$\text{SNR}_{X_i} = P_{(X_i, \xi_i)}/P_{\xi_i}, \tag{7}$$

where , $P_{(X_i, \xi_i)}$ and P_{ξ_i} correspond to the average (normalized) power for the signal and for the noise, respectively. In the three-channel model, the analytical solution for the computation of the signal-to-noise ratio yields (see Supplementary Material, section S1):

$$\text{SNR}_{X_1} = \frac{\pi^2}{3}; \tag{8}$$
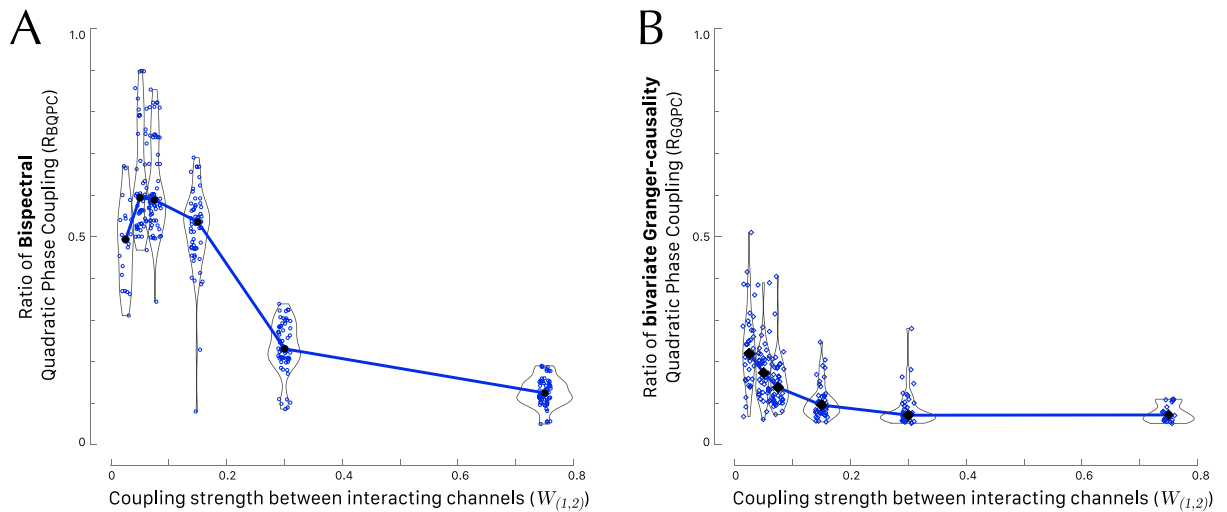
Figure 4. Effect of coupling strength between interacting channels X_1 and X_2 on the method chosen to detect quadratic phase coupling. The curves are centered on the medians of each group. The violin plots show the kernel probability density of the data at different values. (**A**) Ratio of bispectral quadratic phase coupling (R_{BQPC}) as a function of the coupling strength $W_{(1,2)}$ between X_1 and X_2. (**B**) Ratio of bivariate Granger causality Quadratic Phase Coupling (R_{GQPC}) as a function of the coupling strength. For graphical purpose the overlay of points has been limited by adding a random horizontal jitter equal to 0.05.

$$\mathrm{SNR}_{X_2} = 1; \tag{9}$$

$$\mathrm{SNR}_{X_3} = \left(\frac{2}{3}\pi^2 + 2\right) W_{(1,2)}^2 + \frac{1}{2}. \tag{10}$$

In all 354 conditions examined, the SNRs of both experimental time series X_1 and X_2 consistently exceeded their respective expected values (Wilcoxon signed rank test, $p < .001$ for both X_1 and X_2). Conversely, in channel X_3, we observed that for 342 out of 354 conditions, the experimental SNR was consistently smaller than its corresponding expected value (Wilcoxon signed rank test, $p < .001$). This observed effect displayed a non-linear pattern, which was contingent on the coupling strength parameter $W_{(1,2)}$ (Kruskal–Wallis one-way ANOVA $\chi^2_{(5)} = 97.426$, $p < .001$).

The ratio $[SNR_{X_3}]/SNR_{X_3}$ of the experimental SNR divided by its analytical prediction (the expected value of the SNR) can be termed the SNR Efficiency. Higher values of SNR Efficiency (greater than 1) would indicate better-than-expected performance, whereas values less than 1 would suggest inefficiency. Figure 5A plots SNR Efficiency against the coupling strength and shows that SNR Efficiency is consistently underestimated (one-way Welch ANOVA with the coupling weights as factor and SNR Efficiency as dependent variable: $F(5, 150.85) = 10.140$, $p < .001$). The underestimation of the numerical SNR of channel X_3 in comparison with its expected value is rather a positive finding; it indicates that our evaluation of R_{BQPC} or R_{GQPC} as statistics of QPC is favorably conservative. The observed decrease of SNR Efficiency with increasing coupling strength indicates that the discrepancy between the numerical value and its analytically expected counterpart widens as the coupling strength increases. It is noteworthy that the expected value, as derived analytically and detailed in the "Supplementary Material", approaches an asymptotic limit. Conversely, the numerical value is influenced by the intrinsic amplitude of channel X_3, which itself is augmented with an increase in the coupling strength between the interacting channels X_1 and X_2.

The subsequent analysis focused on assessing how the SNR Efficiency in channel X_3 affected the detection of specific QPC by either bispectral analysis or bivariate Granger causality. Figure 5B illustrates that the values of R_{BQPC} consistently surpassed those of R_{GQPC}, regardless of the SNR Efficiency (Wilcoxon signed rank test with continuity correction, $p < .001$ with a large effect size). Kendall's rank correlation test revealed a statistically significant nonlinear dependence between the SNR Efficiency and both the novel specific indices we introduced, namely R_{BQPC} and R_{GQPC}.

Discussion

Quadratic Phase Coupling is essential for uncovering nonlinear interactions and complex relationships within multivariate time series data. Its application spans across multiple fields, including neuroscience, engineering, biology, and signal processing, where understanding nonlinear behaviors is crucial for making meaningful interpretations and improving modeling techniques. QPC can reveal how different brain regions or neurons interact nonlinearly during various cognitive tasks or in different brain states and thus can contribute for advancing our knowledge of brain functional connectivity, as shown in evoked potentials and EEG recordings[40–44], local field potentials[45–47], and magnetoencephalography[46,48]. The current study has introduced a straightforward interaction network model, exemplified by a noisy instantaneous multiplier showcasing characteristic QPC, specific to
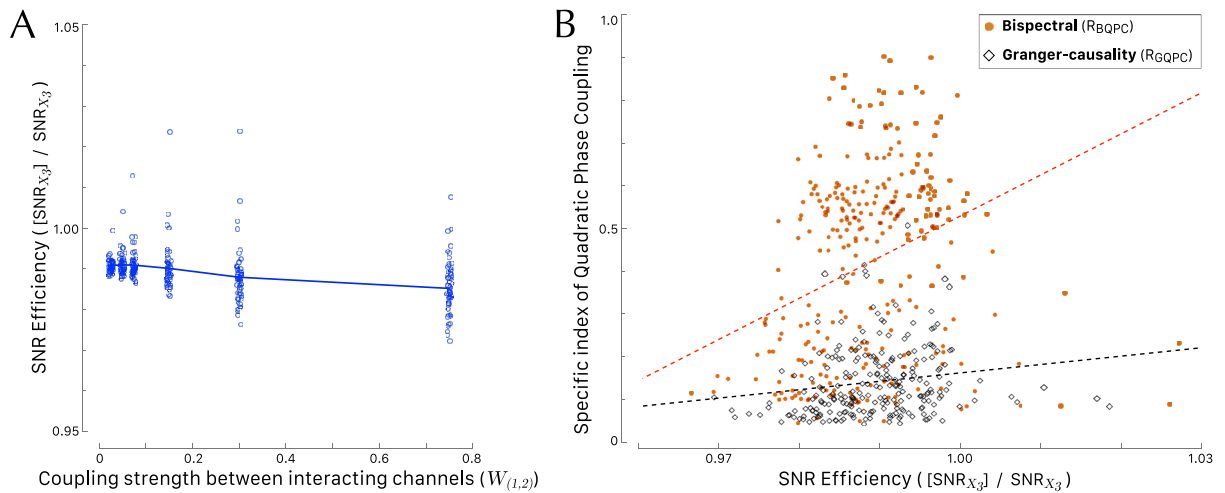
Figure 5. (**A**) Effect of coupling strength between interacting channels X_1 and X_2 on SNR Efficiency of channel X_3. The plot includes the result for all 354 conditions and for graphical purpose the overlay of points has been limited by adding random horizontal and vertical jitters of 0.005 and 0.002, respectively. (**B**) Effect of SNR Efficiency observed in channel X_3 on the novel specific indices of QPC associated with interacting channels X_1 and X_2. The values of R_{BQPC} are generally larger than R_{GQPC} at any value of the SNR Efficiency. The dashed lines correspond to trend lines computed according to Pearson's correlation. For graphical purpose the overlay of points has been limited by adding a random horizontal and vertical jitter equal to 0.008.

the carrying frequencies of the interacting channels. Our investigation revolved around examining bifrequency interactions originating from two channels (X_1, X_2) to a third channel (X_3) within the frequency range of 0–50 Hz range and varying the cross-channel coupling strength from weak to strong.

As the coupling strength between two interacting time series increases, we observe the emergence of spurious values that decrease the value of the new indices R_{BQPC} and R_{GQPC} (Fig. 4). This outcome might seem counter-intuitive at first glance; one would typically expect the coupling parameter to solely enhance the significance of nonlinearity in the third series, X_3, rather than introducing anomalies. Indeed, as anticipated, we do observe increased cross-bicoherence and bivariate Granger causality across a broader band of bifrequencies for larger coupling strengths W(1,2), because these estimators quantify the QPC at any bifrequency (Fig. 3). However, stronger coupling also amplifies the likelihood that non-zero values of the estimators become significant, affecting not only to the signal's component at the carrying frequency but also to the noise components ξ_i, present in the channels X_1 and X_2. These noise components exhibit a constant spectral density, except in the vicinity of the interacting bifrequencies F_1 and F_2. The characteristic of the new indices presented in this study is their dependency on the bispectral specificity of the coupling. Specifically, R_{BQPC} more effectively distinguishes coupling concentrated at a specific bifrequency and coupling distributed over a wider bispectral region than R_{GQPC}.

In interacting networks, linear causal relationships revealed by Granger causality were initially applied in the field of econometrics[28], and extended to study network interactions in biology, for example for determining the preferred direction of gene regulatory networks[49] and metabolic networks[50,51]. However, the nonlinearity within interacting processes makes it difficult to apply parametric approaches for the characterization of recurring processes, such as threshold autoregressive moving average models that have been widely applied to financial time series analysis[52]. Concerns were raised that incorrect conceptual interpretation of causality approaches may lead to highly counterintuitive and potentially misleading results[53]. Observational noise can result in spurious causality detections, prompting the development of more rigorous estimations of Granger causality that have been successfully applied in experimental contexts in recent years[37,54–59]. Bivariate Granger causality, in particular, has proven highly effective in providing insights into how different signals influence each other's phases[48,60]. This type of analysis is especially relevant in neuroscience, where the coupling of oscillatory activities at different frequencies between brain regions is crucial for the formation of functional networks. Other methods specifically sensitive to non-linear interactions (i.e., QPC) were developed and applied to EEG analysis[61,62] However, designations of phase coupling and cross-frequency coupling may be misleading because effects of synchronization should be clearly distinguished from effects of signal transfer (propagation)[41,60,63].

In situations where a signal contains harmonic components or intermodulation (where two or more frequencies mix to create new frequencies), higher-order spectral analyses prove valuable. They help distinguish these components and unveil their interrelationships. An alternative approach to Granger causality, aimed at gaining deeper insights into the characteristics of complex signals that go beyond what traditional power spectra and cross-spectra can reveal, encompasses methods such as the bispectrum and higher-order cumulants. When estimating parameters within the cross-bispectrum, it is assumed that the time series represent realizations of locally stationary processes, even when weak stationarity is present[3,21,25]. This approach relies on the fact that the bispectrum of a linear Gaussian process equals zero. Surrogate data can be used to test the null hypothesis that the original data were generated by a linear Gaussian process and QPC analysis is employed to detect and measure phase coupling that doesn't adhere strictly to linear relationships[64]. To address potential issues related

to mixing artifacts, robust solutions have also been suggested[65]. However, it's important to note that the stationarity condition is a strong assumption. It implies that the probabilistic structure remains unchanged even when there is a significant time shift. This assumption can introduce bias when computing cross-bicoherence[66]. To tackle non-stationarity, wavelet analysis has been employed[7,67]. A specific method, the general harmonic wavelet transform-based bicoherence using phase randomization, was developed to measure the co-modulation of oscillations between different frequency bands at various sleep stages[68]. It's noteworthy that the simultaneous multiplier examined in our current study represents a model of frequency mixers. In this model, channel X_2 plays the role of the local oscillator, assuming that the input of channel X_1 is akin to the input to a mixer. This model, by definition, is stationary. If we view the system generating these processes as a digital filter, then cross-bicoherence analysis reveals the filter's properties. Consequently, our model provides an ideal framework for comparing the accuracy of specific QPC detection between cross-bispectrum and bivariate Granger causality.

The study of neural interactions and their implications for cognitive functions and neurological disorders underscores the importance of detecting specific patterns of QPC. Such detection is crucial for neuroscience applications aimed at better understanding the temporal and spatial coordination between different brain regions. In clinical neuroscience research, identifying aberrant QPC patterns, such as in the study of epilepsy, could help pinpoint the epileptogenic zones responsible for initiating and propagating seizure activity[13,44,69–71]. This information is critical for guiding surgical interventions or developing targeted neuromodulation therapies. Similarly, in Alzheimer's disease, altered QPC patterns could serve as early biomarkers for disease progression or indicators of therapeutic intervention efficacy, thereby aiding in early diagnosis and the evaluation of treatments[45,72–74]. In the future, the detection of QPC could play a key role in neurorehabilitation, where understanding the reorganization of neural networks following injury or in response to therapy is paramount. Analyzing changes in QPC patterns in EEG or magnetoencephalography recordings before and after rehabilitation interventions could assess the neural basis of recovery and functional improvement, potentially leading to more personalized and effective rehabilitation strategies. Furthermore, by identifying specific QPC patterns from participants engaged in tasks requiring sustained attention or memory manipulation, the brain rhythms and dynamic networks activated during these cognitive processes could be elucidated.

In conclusion, cross-bicoherence is a valuable tool for detecting and quantifying phase coupling in multivariate time series data, especially in situations where nonlinear interactions are expected. We presented a simple model exemplifying how higher-order spectral analysis helps identify and mitigate interference, and enhance the detection of weak signals in noisy environments. QPC can uncover hidden patterns or relationships that might be missed by linear methods and an innovative computational approach was developed to evaluate the accuracy of QPC detection using different and complementary approaches. Our results revealed that cross-bicoherence, in comparison to a similar metric derived from bivariate Granger causality, offers several advantages. Notably, cross-bicoherence exhibits enhanced capability in detecting specific QPC resulting from the weak coupling of the interacting channels, demonstrating greater robustness against input noise.

Methods
Cross-bicoherence analysis
In this work, we consider a three-dimensional real vector X at time t as a particular multivariate time series or a realization of stochastic process that has polyspectra[1,3,75],

$$X(t) = \begin{bmatrix} X_i(t) \\ X_j(t) \\ X_k(t) \end{bmatrix}$$

where $X_i(t)$, $X_j(t)$, and $X_k(t)$ are three time series comparable to experimental brain signals. In particular, let us assume that $X(t)$ is jointly stationary over the time period of observation and $\tilde{X}_i(f)$, $\tilde{X}_j(f)$, and $\tilde{X}_k(f)$ are the corresponding discrete Fourier transform at frequency f of each time series. After an appropriate preprocessing if necessary, we can assume that each time series is of mean $\mu = 0$ and variance $\sigma^2 = 1$ without loss of generality. For any two time series $X_i(t)$, $X_j(t)$, the cross-spectrum at frequency f is estimated by:

$$\hat{C}_{ij}(f) = \tilde{X}_i(f)\tilde{X}_j^*(f) \tag{11}$$

where the superscript (*) stands for the complex conjugate transpose. For a single time series $X_i(t)$, the *bispectrum* at two frequencies f_1 and f_2 is estimated by:

$$\hat{B}_i(f_1, f_2) = \tilde{X}_i(f_1)\tilde{X}_i(f_2)\tilde{X}_i^*(f_1 + f_2). \tag{12}$$

For a three-dimensional time series $X(t)$, the *cross-bispectrum* at frequencies f_1 for X_i and f_2 for X_j is estimated by the third joint moments of these processes:

$$\hat{B}_{ijk}(f_1, f_2) = \tilde{X}_i(f_1)\tilde{X}_j(f_2)\tilde{X}_k^*(f_1 + f_2) \tag{13}$$

The sample statistics of the magnitude-squared cross-bicoherence $\hat{b}_{ijk}^2$ simply referred to as *cross-bicoherence*, is a normalization of the cross-bispectrum as follows, where $\langle \cdot \rangle$ denotes the sample average (i.e., expected value of the sample):

$$\hat{b}_{ijk}^2(f_1,f_2) = \frac{\left\langle \left| \hat{B}_{ijk}(f_1,f_2) \right|^2 \right\rangle}{\left\langle \left| \tilde{X}_i(f_1)\tilde{X}_j(f_2) \right|^2 \right\rangle \left\langle \left| \tilde{X}_k^*(f_1+f_2) \right|^2 \right\rangle}. \tag{14}$$

It always holds that $0 \leq \hat{b}_{ijk}^2(f_1,f_2) \leq 1$ as the Cauchy–Schwarz inequality guarantees the upper bound. The values of *cross-bicoherence* can be used to interpret the interaction of X_i and X_j on X_k (i.e., how well X_k corresponds to X_i and X_j) at each bifrequencies pair (f_1,f_2). The estimation method used in the present work has been implemented and publicly available as an R package called `rhosa`[76]. Notice that the distribution of the estimated bicoherence converges to a noncentral χ^2 distribution, if the null hypothesis holds that its genuine value is zero[77]. Furthermore, it can be approximated by a χ^2 distribution[24].

Estimation of a significance threshold based on the false discovery rate
We introduce a novel estimation of significant non-zero cross-bicoherence based on the false discovery rate (FDR) approach[78–80]. The estimation of significant non-zero cross-bicoherence is done on a large number of bins and a usual Type I Error equivalent to a confidence level of 95% ($p = 0.05$) would imply that 5% of all tests result in false positives. While $p = 0.05$ is acceptable for one test, it is not in case of a multiple testing problem. In FDR, q-values (or adjusted p-values) are determined for the tests that result in a discovery (i.e., a significant result), such that $q = 0.05$ implies that 5% of significant tests (and not 5% of all tests) will result in false positives. Then, a cutoff $q = 0.05$ will result in fewer false positives than a cutoff $p = 0.05$.

In our novel procedure, we fit a two-class mixture distribution to the raw values of the cross-bicoherence for a given q-value. Assuming that F is the probability density of the cross-bicoherence in the trapezoidal domain of bifrequencies, we sought

$$F(x) = p_0 F_0(x) + [1 - p_0]F_A(x) \tag{15}$$

where $F_0(x)$ is a χ^2 distribution following the null hypothesis of zero cross-bicoherence; $F_A(x)$ is an alternative distribution; p_0 is the fraction of the statistic governed by the null hypothesis. The fitting is done by the mode matching method[81] (which also provides a one-side test of the (positive) right-tail FDR against the empirical null distribution), with a fitting interval $p_0 = [0, 0.9]$ and bin width $\Delta = 0.001$. Hence, we denote $\overline{b}_{ijk}^2(f_1,f_2)$ the non-zero estimated cross-bicoherences significant to FDR with the assumption of a threshold $q = 0.05$ of FDR for each significance testing.

Ratio of bispectral quadratic phase coupling (R_{BQPC})
In a quadratic system, QPC occurs when the second-order nonlinearities of interacting $X_i(t)$ and $X_j(t)$ at bifrequencies (f_1,f_2) (for X_i and X_j, respectively) contribute to the power of $X_k(t)$. Given the symmetries in the distorted hexagonal cross-bicoherence domain[82–84] (Fig. 6A), the QPC must be observed in the corresponding sector $Q(f_1,f_2)$ if the sum of the two interacting frequencies exceeds the Nyquist frequency (i.e., $f_1 + f_2 > f_{Nyquist}$). According to the three mutually exclusive conditions on bifrequencies (f_1,f_2), the sectors $Q(f_1,f_2)$ are defined as follows (Fig. 6B):

$$Q(f_1,f_2) = \begin{cases} Q_I & \text{if } (f_1+f_2) \leq f_{Nyquist}; \\ Q_{II} & \text{if } (f_1+f_2) > f_{Nyquist} \text{ and } f_1 > f_2; \\ Q_{III} & \text{if } (f_1+f_2) > f_{Nyquist} \text{ and } f_1 \leq f_2. \end{cases}$$
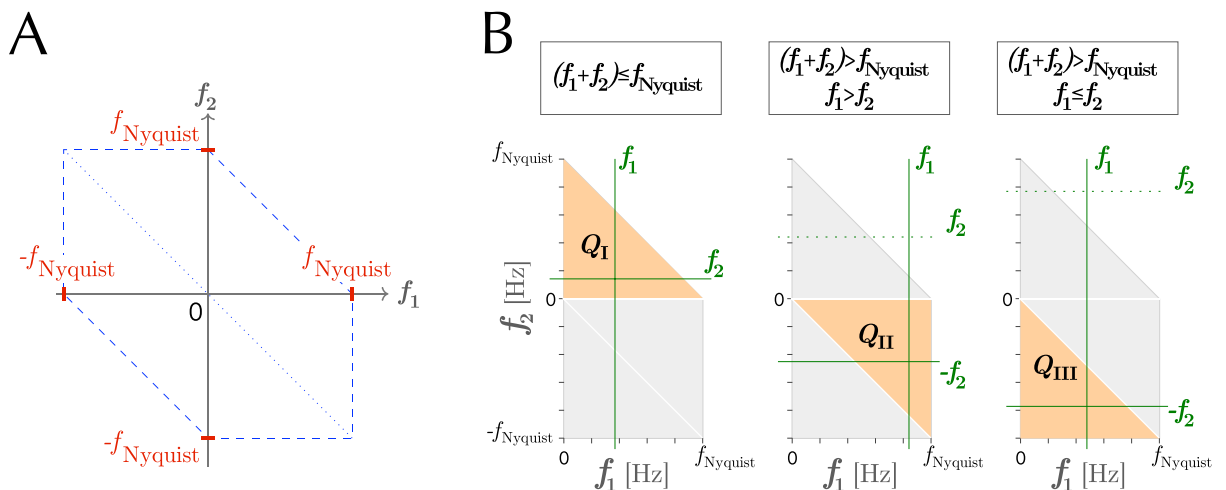
Figure 6. (**A**) The domain of cross-bicoherence corresponds to the distorted hexagon, surrounded by dashed lines. (**B**) The three sectors Q_I, Q_{II}, and Q_{III} in the principal domain of cross-bicoherence of real-valued time series.

The accuracy of experimental recordings is generally limited by the fact that measurements of brain activity is indirect. Small time delays and shifts in frequencies may be artificially produced by the recording techniques. Hence, an interaction occurring at bifrequencies (f_1, f_2) is extended to a neighborhood of interest $G(f_1, f_2; d)$, such that $g_1 \in [f_1 - d, f_1 + d]$ and $g_2 \in [f_2 - d, f_2 + d]$, defined by the positive value d in frequency unit.

We introduce a novel index designed to quantify the quadratic phase coupling in the bispectral domain that is specifically associated with the carrying frequencies of the input signals from interacting channels. This index is distinct from a generic estimator, which can be influenced by significant non-zero values that are affected by noise components, ξ_1 and ξ_2, present in those channels. The ratio of bispectral quadratic phase coupling $R_{\text{BQPC}}(f_1, f_2; d)$ is defined as the numerical integration of significant (i.e., $q \leq 0.05$) cross-bicoherences in the neighborhood of interest divided by *all* significant cross-bicoherences in the relevant sector of bifrequencies (i.e., $(g_1, g_2) \in Q(f_1, f_2)$):

$$R_{\text{BQPC}}(f_1, f_2; d) = \frac{\displaystyle\sum_{(g_1, g_2) \in G(f_1, f_2; d)} \overline{b_{ijk}^2}(g_1, g_2)}{\displaystyle\sum_{(g_1, g_2) \in Q(f_1, f_2)} \overline{b_{ijk}^2}(g_1, g_2)}. \tag{16}$$

Notice that $G(f_1, f_2; d) \subset Q(f_1, f_2)$ and $R_{\text{BQPC}}(f_1, f_2; d)$ is upper bounded to 1.

The frequency range (or bandwidth) of the spectrum is determined by the sampling frequency and, for a given sampling frequency, the spectral resolution Δf (or resolution frequency) is determined by the number of points acquired in the recorded time series[85,86]. For example, an experiment acquiring 500 points at 100 Hz would yield an experimental frequency resolution $\Delta f = 100/500$ Hz, i.e. $\Delta f = 0.2$ Hz. Then, an actual frequency resolution $\Delta f = 0.25$ Hz in the bispectral domain of cross-bicoherence was determined as being the closest fractional value of power two.

This computation is illustrated by the analysis of a test data set formed by three artificially generated time series (X_1, X_2, X_3), recorded from 128 simulation runs of 5 seconds epochs sampled at 100 Hz. For time series formed by merging multiple epochs of the same duration, the Welch's approach to frequency domain estimations is applied[87] with an overlap of 50% for two consecutive data epochs. In this example, each time series is driven by a distinct periodic input ($F_1 = 8.5$ Hz, $F_2 = 10.5$ Hz, $F_3 = 9.5$ Hz) and the sources are interconnected. In particular, we compute $R_{\text{BQPC}}(f_1, f_2; d)$ with $R_{\text{BQPC}}(8.5, 10.5; 0.5)$ (i.e. a neighborhood of interest of 0.5 Hz around each frequency that participates to the interaction). In this case, the interaction occurs in the sector Q_{I} (Fig. 7A). The estimation of a significance threshold based on FDR allows to plot a cross-bicoherence significance map (Fig. 7B) showing all bifrequencies characterized by cross-bicoherence values different from zero ($\overline{b_{ijk}^2}$). In this example, the sum of all significant cross-bicoherences in the sector Q_{I} is equal to $\sum_{(g_1, g_2) \in Q(8.5, 10.5)} \overline{b_{ijk}^2}(g_1, g_2) = 10.906$ (Fig. 7C). We considered the bifrequencies neighborhood of interest $G(f_1 \in [8, 9], f_2 \in [10, 11])$. The sum of all significant cross-bicoherences in this neighborhood of interest is equal to $\sum_{(g_1, g_2) \in G(8.5, 10.5; 0.5)} \overline{b_{ijk}^2}(g_1, g_2) = 3.604$ (Fig. 7D). Hence, in this example $R_{\text{BQPC}} = 3.604/10.906 = 0.330$.

Bivariate Granger causality in the frequency-domain
In the time-domain, the unconditional GC yields information on the strength of the causal dependency between two time series $X_i(t)$ and $X_j(t)$[30,33]. The GC of X_j on X_i compares a first model where the value of X_i at time t is a linear weighted sum of its own past history (i.e., a linear vector autoregressive model, VAR)

$$X_i(t) = \sum_{m=1}^{p} a_m X_i(t - m) + \varepsilon_t \tag{17}$$

with a second model where the value of X_i at time t is a linear weighted sum of its own and of X_j histories

$$X_i(t) = \sum_{m=1}^{q} b_m X_i(t - m) + \sum_{m=1}^{q} c_m X_j(t - m) + \eta_t \tag{18}$$

where p and q are the lag orders of two models, and a_m, b_m, c_m are real coefficients of the VARs, and η_t, ε_t are terms corresponding to the residual errors. In other words, the GC of X_j on X_i measures if past values of X_j yield information that predicts the next X_i values better than solely the past X_i history does.

In the frequency-domain, the Fourier representations of multivariate time series $X(t)$ can be used to define GC with a spectral decomposition under some regularity conditions[88]. Let $\text{GCS}(X_i, X_j, f)$ denote the spectral GC of X_i on X_j at frequency f. For a bivariate stochastic process $X_{ij}(t) = [X_i(t), X_j(t)]$ (defined as the point-wise product of $X_i(t)$ and $X_j(t)$ at each time step t) in presence of a third time series $X_k(t)$, it is possible to extend the GC in the frequency-domain by defining the unconditional bivariate GC spectrum $\text{BGCS}_{ij \to k}(f) = \text{GCS}(X_i X_j, X_k, f)$. It measures the strength of the causal dependency of X_{ij} on X_k.

In our practical implementation, the parameters of the vector autoregressive models (VAR(l) models) are computed using the `vars` R package[89]. The VAR's lag order l is selected according to the Schwarz Criterion (SC) (also called Bayesian information criterion, BIC)[90] among other criteria because it offers the best probability of choosing the simplest possible model for large time series[91]. In principle, the smaller the SC value the better the fit of the model. However, very long time series are more likely to be overfitted and large lag orders could be
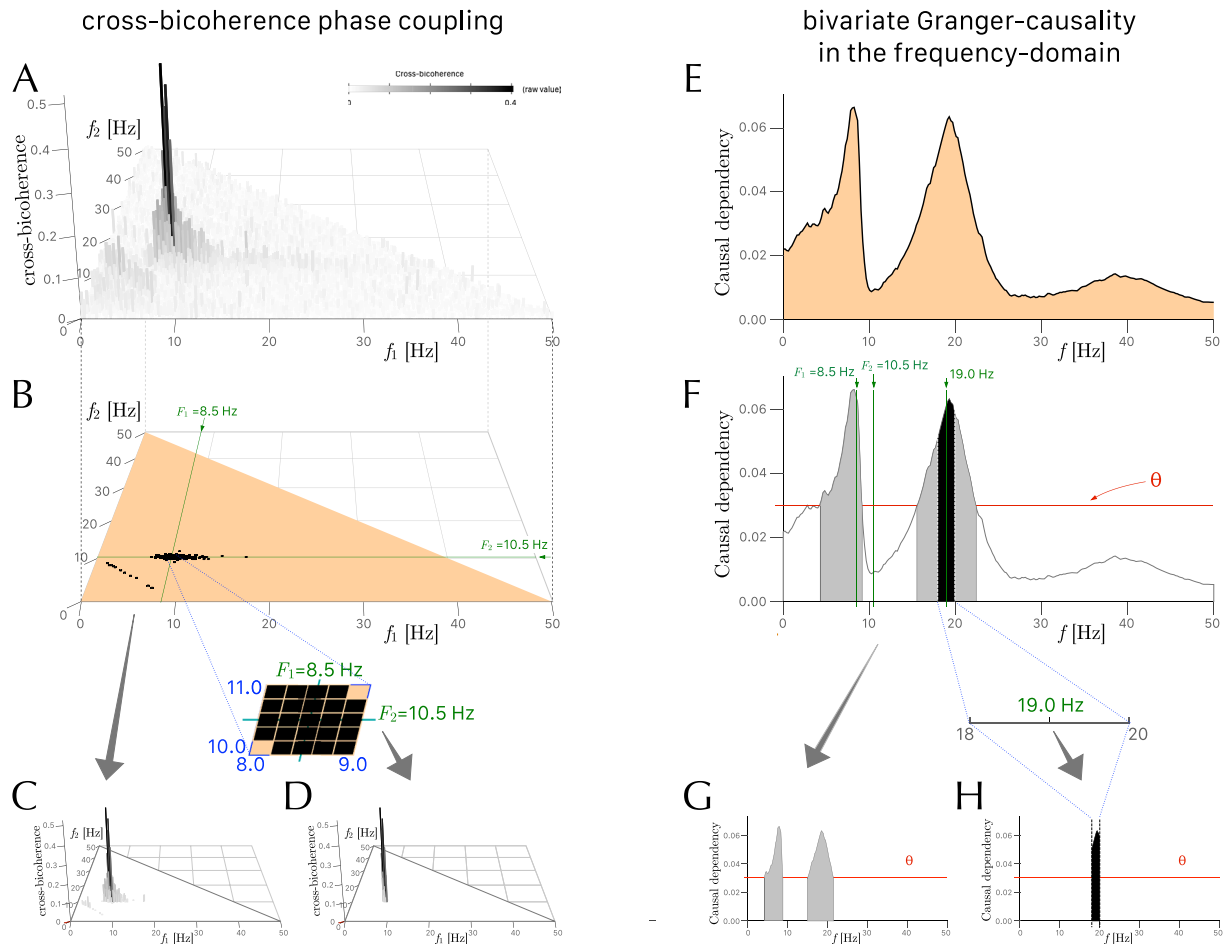
Figure 7. Three time series X_1, X_2, X_3 are recorded simultaneously (see text for more details). Estimation of the effect of quadratic phase coupling between X_1, X_2 for interacting bifrequencies ($F_1 = 8.5\,\text{Hz}$, $F_2 = 10.5\,\text{Hz}$) on X_3. The panels on the left side refer to the evaluation of the cross-bicoherence phase coupling and the panels on the right side refer to the evaluation of the bivariate Granger causality in the frequency-domain. (**A**) All cross-bicoherence values are computed in the sector Q_I. (**B**) The cross-bicoherence significance map, showing all bifrequencies (black bins) characterized by significant cross-bicoherence values. (**C**) The cross-bicoherence plot, showing all significant cross-bicoherence values whose sum is equal to 10.906 in this example. (**D**) The cross-bicoherence plot for the bifrequencies neighborhood of interest ($f_1 \in [8, 9]$, $f_2 \in [10, 11]$) (enlargement centered at a green cross mark), shows that the sum of these significant values is equal to 3.604, which yields $R_{\text{BQPC}} = 0.330$ (i.e., 3.604/10.906). (**E**) For the same data, the median unconditional bivariate GC spectrum measures the strength of the causal dependency of the bivariate process $X_{1,2}$ on X_3 computed with the optimal VAR's lag model, that is a VAR(7) model in this example. (**F**) A threshold value $\theta = 0.0301$ is calculated to determine the significant values of Granger causality in the frequency domain. (**G**) The integration over the curve shows that the sum of all significant values is equal to 0.552. (**H**) For the spectral interval of interest ($f \in [18, 20]$), the sum of all significant values is equal to 0.128, which yields $R_{\text{GQPC}} = 0.233$ (i.e., 0.128/0.552).

incorrectly selected: the lowest SC value could be associated with lag orders without giving much more information about model fit. Hence, an heuristic approach is aimed to avoid overfitting: instead of choosing the VAR's lag order l corresponding to the lowest SC, we select the lag order l corresponding to 95% of the lowest SC value with parameter `lag.max = 50`.

The estimation of $\text{BGCS}_{ij \to k}$ follows the bootstrap method as implemented in `grangers` R package[34]. The `nboots` parameter (corresponding to the number of bootstrap series) is determined following the experimental spectral resolution Δf, i.e. `nboots` $= \sqrt{\Delta f} \times 1000$. We estimate the q-values of FDR from the set of p-values simultaneously calculated for all of Fourier frequencies in $(0, f_{\text{Nyquist}})$, using the R package called `qvalue` and setting the parameter `pfdr = TRUE` for a more robust FDR estimation[92,93]. In case the variance of bootstrapped p-values is too small, the Benjamini-Hochberg procedure is used as a conservative alternative by setting the parameter `lambda = 0` for an estimation of the proportion of true null p-values. Following the FDR level of significance $q < .05$ for $\text{BGCS}_{ij \to k}$, we compute the value of causal dependency corresponding to the threshold θ which determines the significant values of the bivariate GC spectrum. With the Welch's approach (with 50% overlap) for time series formed by merging multiple epochs of same duration, we compute the median $\text{BGCS}_{ij \to k}$ and the median value of threshold θ across all Welch's data segments.

Ratio of bivariate Granger causality quadratic phase coupling (R_{GQPC})

Following the same approach determining R_{BQPC}, we consider QPC occurring when a nonlinear interaction between $X_i(t)$ and $X_j(t)$ at bifrequencies (f_1, f_2) produces a peak at frequency f in the unconditional bivariate GC spectrum $BGCS_{ij \to k}(f)$ computed for the optimal VAR's lag order l. For an extension to experimental data, we consider the interaction at frequency f (determined by bifrequencies (f_1, f_2)) occurring within a spectral interval of interest $(f_1, f_2; d)$ (similar to the neighborhood of interest for the cross-bicoherence). Then, $f \in [(f_1 + f_2) - 2d, (f_1 + f_2) + 2d]$ if $(f_1 + f_2) \leq f_{Nyquist}$ and $f \in [f_{Nyquist} - (f_1 + f_2) - 2d, f_{Nyquist} - (f_1 + f_2) + 2d]$ if $(f_1 + f_2) > f_{Nyquist}$ because of aliasing.

We introduce a novel index designed to quantify the quadratic phase coupling associated with Granger causality in a specific bivariate process. This index focuses on the carrying frequencies of the interacting channels, X_1 and X_2. The ratio of bivariate Granger causality quadratic phase coupling $R_{GQPC}(f_1, f_2; d)$ is defined by the fraction of causal effects of the bivariate process X_{ij} at a frequency f given $X_k(t)$:

$$R_{GQPC}(f_1, f_2; d) = \frac{\sum_{f \in (f_1, f_2; d)} \overline{BGCS_{ij \to k}}(f)}{\sum_{f \in [0, f_{Nyquist}]} \overline{BGCS_{ij \to k}}(f)}. \tag{19}$$

where $\overline{BGCS_{ij \to k}}(f)$ is the significantly non-zero value of the bivariate GC spectrum from X_{ij} to X_k at frequency f. Notice that $R_{GQPC}(f_1, f_2; d)$ is upper bounded to 1.

This is illustrated in Fig. 7 using the same time series used to illustrate the computations for the cross-bicoherence. The median unconditional bivariate GC spectrum is calculated with a VAR(7) model, (i.e. VAR's lag order $l = 7$) and `nboots` = 447 (Fig. 7E). For this example, the median threshold value of 113 Welch's data segments of 500 data points each is $\theta = 0.0301035$ (Fig. 7F). The sum of all significant values of unconditional GC is equal to $\sum_{f \in (f_1, f_2; d)} \overline{BGCS_{1,2 \to 3}}(f) = 0.552$ (Fig. 7G). The spectral interval of interest of the unconditional GC spectrum ($f \in [18, 20]$) is determined by bifrequencies ($f_1 = 8.5, f_2 = 10.5$). The sum of all significant values of unconditional GC in this spectral interval is equal to $\sum_{f \in (f_1, f_2; d)} \overline{BGCS_{1,2 \to 3}}(f) = 0.128$ (Fig. 7H). In this example $R_{GQPC} = 0.128/0.552 = 0.233$.

Data availibility

The time series that support the results of this study are available from the corresponding author upon reasonable request.

References

1. Brillinger, D. R. An introduction to polyspectra. *Ann. Math. Stat.* **36**, 1351–1374. https://doi.org/10.1214/aoms/1177699896 (1965).
2. Rosenblatt, M. & Ness, J. W. V. Estimation of the bispectrum. *Ann. Math. Stat.* **36**, 1120–1136. https://doi.org/10.1214/aoms/1177699987 (1965).
3. Brillinger, D. R. & Rosenblatt, M. Asymptotic theory of estimates of kth-order spectra. *Proc. Natl. Acad. Sci. U. S. A.* **57**, 206–10. https://doi.org/10.1073/pnas.57.2.206 (1967).
4. Huber, P., Kleiner, B., Gasser, T. & Dumermuth, G. Statistical method for phase investigating relations in stationary stochastic processes. *IEEE Trans. Audio Electroacoust.* **19**, 78–86. https://doi.org/10.1109/TAU.1971.1162163 (1971).
5. Ivanov, P. C. *et al.* Scaling behaviour of heartbeat intervals obtained by wavelet-based time-series analysis. *Nature* **383**, 323–7. https://doi.org/10.1038/383323a0 (1996).
6. Frangakis, A. S., Stoschek, A. & Hegerl, R. Wavelet transform filtering and nonlinear anisotropic diffusion assessed for signal reconstruction performance on multidimensional biomedical data. *IEEE Trans. Biomed. Eng.* **48**, 213–22. https://doi.org/10.1109/10.909642 (2001).
7. Li, X., Yao, X., Fox, J. & Jefferys, J. G. Interaction dynamics of neuronal oscillations analysed using wavelet transforms. *J. Neurosci. Methods* **160**, 178–85. https://doi.org/10.1016/j.jneumeth.2006.08.006 (2007).
8. Taplidou, S. A. & Hadjileontiadis, L. J. Nonlinear analysis of wheezes using wavelet bicoherence. *Comput. Biol. Med.* **37**, 563–70. https://doi.org/10.1016/j.compbiomed.2006.08.007 (2007).
9. Rummel, C. *et al.* Uniform approach to linear and nonlinear interrelation patterns in multivariate time series. *Phys. Rev. E Stat. Nonlinear Soft Matter Phys.* **83**, 066215. https://doi.org/10.1103/PhysRevE.83.066215 (2011).
10. DiRienzo, A. G., Zurbenko, I. G. & Carpenter, D. O. Time series analysis of Aplysia total motion activity. *Biometrics* **54**, 493–508. https://doi.org/10.2307/310975810.2307/3109758 (1998).
11. José, M. V. & Bishop, R. F. Scaling properties and symmetrical patterns in the epidemiology of rotavirus infection. *Philos. Trans. R. Soc. Lond. B Biol. Sci.* **358**, 1625–41. https://doi.org/10.1098/rstb.2003.1291 (2003).
12. Skardal, P. S. & Arenas, A. Higher order interactions in complex networks of phase oscillators promote abrupt synchronization switching. *Commun. Phys.* **3**, 218. https://doi.org/10.1038/s42005-020-00485-0 (2020).
13. Bullock, T. H., Achimowicz, J. Z., Duckrow, R. B., Spencer, S. S. & Iragui-Madoz, V. J. Bicoherence of intracranial EEG in sleep, wakefulness and seizures. *Electroencephalogr. Clin. Neurophysiol.* **103**, 661–678. https://doi.org/10.1016/s0013-4694(97)00087-4 (1997).
14. Schanze, T. & Eckhorn, R. Phase correlation among rhythms present at different frequencies: Spectral methods, application to microelectrode recordings from visual cortex and functional implications. *Int. J. Psychophysiol.* **26**, 171–189. https://doi.org/10.1016/s0167-8760(97)00763-0 (1997).
15. Ning, T. & Bronzino, J. D. Quadratic phase coupling as a quantitative measure for the developing hippocampal formation. *Ann. Biomed. Eng.* **26**, 688–693. https://doi.org/10.1114/1.43 (1998).
16. Perrig, S. *et al.* Changes in quadratic phase coupling of EEG signals during wake and sleep in two chronic insomnia patients, before and after cognitive behavioral therapy. *Front. Artif. Intell. Appl.* **204**, 217–228. https://doi.org/10.3233/978-1-60750-072-8-217 (2009).

17. Schiecke, K., Eiselt, M., Schlattmann, P. & Witte, H. Quadratic phase couplings in the EEG of premature and full-term newborn during quiet sleep. *Methods Inf. Med.* **54**, 205–8. https://doi.org/10.3414/ME13-02-0046 (2015).

18. Coelli, S. *et al.* Higher order spectral analysis of scalp EEG activity reveals non-linear behavior during rhythmic visual stimulation. *J. Neural Eng.* **16**, 056028. https://doi.org/10.1088/1741-2552/ab296e (2019).

19. Bai, Y., Xia, X., Wang, Y., He, J. & Li, X. Electroencephalography quadratic phase self-coupling correlates with consciousness states and restoration in patients with disorders of consciousness. *Clin. Neurophysiol.* **130**, 1235–1242. https://doi.org/10.1016/j.clinph.2019.04.710 (2019).

20. Tacchino, G., Coelli, S., Reali, P., Galli, M. & Bianchi, A. M. Bicoherence interpretation in EEG requires signal to noise ratio quantification: An application to sensorimotor rhythms. *IEEE Trans. Biomed. Eng.* **67**, 2696–2704. https://doi.org/10.1109/TBME.2020.2969278 (2020).

21. Raghuveer, M. & Nikias, C. Bispectrum estimation: A parametric approach. *IEEE Trans. Acoust.* **33**, 1213–1230. https://doi.org/10.1109/TASSP.1985.1164679 (1985).

22. Ning, T. & Bronzino, J. D. Autoregressive and bispectral analysis techniques: EEG applications. *IEEE Eng. Med. Biol. Mag.* **9**, 47–50. https://doi.org/10.1109/51.62905 (1990).

23. Fackrell, J. & McLaughlin, S. Quadratic phase coupling detection using higher order statistics. In *IEE Colloquium on Higher Order Statistics in Signal Processing: Are They of Any Use?* Vol. 9, 1–8, https://doi.org/10.1049/ic:19950736 (1995).

24. Elgar, S. & Sebert, G. Statistics of bicoherence and biphase. *J. Geophys. Res.* **94**, 10993–10998. https://doi.org/10.1029/JC094iC08p10993 (1989).

25. Brillinger, D. & Irizarry, R. An investigation of the second- and higher-order spectra of music. *Signal Process.* **65**, 161–179. https://doi.org/10.1016/S0165-1684(97)00217-X (1998).

26. Sommerlade, L. *et al.* Optimized spectral estimation for nonlinear synchronizing systems. *Phys. Rev. E Stat. Nonlinear Soft Matter Phys.* **89**, 032912. https://doi.org/10.1103/PhysRevE.89.032912 (2014).

27. Siu, K. L. *et al.* Statistical approach to quantify the presence of phase coupling using the bispectrum. *IEEE Trans. Biomed. Eng.* **55**, 1512–1520. https://doi.org/10.1109/TBME.2007.913418 (2008).

28. Granger, C. W. J. Investigating causal relations by econometric models and cross-spectral methods. *Econometrica* **37**, 424–438. https://doi.org/10.2307/1912791 (1969).

29. Winterhalder, M. *et al.* Comparison of linear signal processing techniques to infer directed interactions in multivariate neural systems. *Signal Process.* **85**, 2137–2160. https://doi.org/10.1016/j.sigpro.2005.07.011 (2005).

30. Geweke, J. Measurement of linear dependence and feedback between multiple time series. *J. Am. Stat. Assoc.* **77**, 304–313. https://doi.org/10.1080/01621459.1982.10477803 (1982).

31. Diks, C. & Panchenko, V. A new statistic and practical guidelines for nonparametric Granger causality testing. *J. Econ. Dyn. Control* **30**, 1647–1669. https://doi.org/10.1016/j.jedc.2005.08.008 (2006).

32. Geweke, J. Measures of conditional linear dependence and feedback between time series. *J. Am. Stat. Assoc.* **79**, 907–915. https://doi.org/10.1080/01621459.1984.10477110 (1984).

33. Chen, Y., Bressler, S. L. & Ding, M. Frequency decomposition of conditional Granger causality and application to multivariate neural field potential data. *J. Neurosci. Methods* **150**, 228–237. https://doi.org/10.1016/j.jneumeth.2005.06.011 (2006).

34. Farnè, M. & Montanari, A. A bootstrap method to test Granger-causality in the frequency domain. *Comput. Econ.* **59**, 935–966. https://doi.org/10.1007/s10614-021-10112-x (2022).

35. Ding, M., Chen, Y. & Bressler, S. L. Granger causality: Basic theory and application to neuroscience. In *Handbook of Time Series Analysis* (eds Schelter, B. *et al.*) 437–460 (Wiley, Hoboken, 2006). https://doi.org/10.1002/9783527609970.ch17.

36. Breitung, J. & Schreiber, S. Assessing causality and delay within a frequency band. *Econ. Stat.* **6**, 57–73. https://doi.org/10.1016/j.ecosta.2017.04.005 (2018).

37. Li, Y., Lei, M., Cui, W., Guo, Y. & Wei, H.-L. A parametric time-frequency conditional Granger causality method using ultra-regularized orthogonal least squares and multiwavelets for dynamic connectivity analysis in EEGs. *IEEE Trans. Biomed. Eng.* **66**, 3509–3525. https://doi.org/10.1109/tbme.2019.2906688 (2019).

38. Barnett, L. & Seth, A. K. The MVGC multivariate Granger causality toolbox: A new approach to Granger-causal inference. *J. Neurosci. Methods* **223**, 50–68. https://doi.org/10.1016/j.jneumeth.2013.10.018 (2014).

39. Hidalgo, J. A bootstrap causality test for covariance stationary processes. *J. Econom.* **126**, 115–143. https://doi.org/10.1016/j.jeconom.2004.02.009 (2005).

40. Samar, V. *et al.* Quadratic phase coupling in auditory evoked potentials from healthy old subjects and subjects with Alzheimer's dementia. In *[1993 Proceedings] IEEE Signal Processing Workshop on Higher-Order Statistics*, 361–365, https://doi.org/10.1109/HOST.1993.264535 (1993).

41. Witte, H. & Schack, B. Quantification of phase coupling and information transfer between electroencephalographic (EEG) signals: Analysis strategies, models and simulations. *Theory Biosci.* **122**, 361–381. https://doi.org/10.1078/1431-7613-00095 (2003).

42. Schwab, K., Putsche, P., Eiselt, M., Helbig, M. & Witte, H. On the rhythmicity of quadratic phase coupling in the tracé alternant EEG in healthy neonates. *Neurosci. Lett.* **369**, 179–82. https://doi.org/10.1016/j.neulet.2004.05.053 (2004).

43. Perrig, S. *et al.* Functional interactions in hierarchically organized neural networks studied with spatiotemporal firing patterns and phase-coupling frequencies. *Chin. J. Physiol.* **53**, 382–395. https://doi.org/10.4077/CJP.2010.AMM039 (2010).

44. Villa, A. E. P. & Tetko, I. V. Cross-frequency coupling in mesiotemporal EEG recordings of epileptic patients. *J. Physiol. Paris* **104**, 197–202. https://doi.org/10.1016/j.jphysparis.2009.11.024 (2010).

45. Villa, A. E. P., Tetko, I. V., Dutoit, P. & Vantini, G. Non-linear cortico–cortical interactions modulated by cholinergic afferences from the rat basal forebrain. *Biosystems* **58**, 219–228. https://doi.org/10.1016/s0303-2647(00)00126-x (2000).

46. Avarvand, F. S. *et al.* Localizing bicoherence from EEG and MEG. *Neuroimage* **174**, 352–363. https://doi.org/10.1016/j.neuroimage.2018.01.044 (2018).

47. Li, Z., Dong, Z., Bai, X. & Liu, M. Characterizing the orientation selectivity in V1 and V4 of macaques by quadratic phase coupling. *J. Neural Eng.* **17**, 036028. https://doi.org/10.1088/1741-2552/ab9843 (2020).

48. Marzetti, L. *et al.* Brain functional connectivity through phase coupling of neuronal oscillations: A perspective from magnetoencephalography. *Front. Neurosci.* **13**, 964. https://doi.org/10.3389/fnins.2019.00964 (2019).

49. Finkle, J. D., Wu, J. J. & Bagheri, N. Windowed Granger causal inference strategy improves discovery of gene regulatory networks. *Proc. Natl. Acad. Sci. U. S. A.* **115**, 2252–2257. https://doi.org/10.1073/pnas.1710936115 (2018).

50. Walther, D., Strassburg, K., Durek, P. & Kopka, J. Metabolic pathway relationships revealed by an integrative analysis of the transcriptional and metabolic temperature stress-response dynamics in yeast. *OMICS* **14**, 261–74. https://doi.org/10.1089/omi.2010.0010 (2010).

51. Wang, L., Sun, X., Weiszmann, J. & Weckwerth, W. System-level and Granger network analysis of integrated proteomic and metabolomic dynamics identifies key points of grape berry development at the interface of primary and secondary metabolism. *Front. Plant Sci.* **8**, 1066. https://doi.org/10.3389/fpls.2017.01066 (2017).

52. Chen, C. W. S., Liu, F.-C. & So, M. K. P. A review of threshold time series models in finance. *Stat. Interface* **4**, 167–181. https://doi.org/10.4310/SII.2011.v4.n2.a12 (2011).

53. Stokes, P. A. & Purdon, P. L. A study of problems encountered in Granger causality analysis from a neuroscience perspective. *Proc. Natl. Acad. Sci. U. S. A.* **114**, E7063–E7072. https://doi.org/10.1073/pnas.1704663114 (2017).

54. Sommerlade, L. *et al.* Assessing the strength of directed influences among neural signals: An approach to noisy data. *J. Neurosci. Methods* **239**, 47–64. https://doi.org/10.1016/j.jneumeth.2014.09.007 (2015).

55. Hu, S. *et al.* Comparison analysis: Granger causality and new causality and their applications to motor imagery. *IEEE Trans. Neural Netw. Learn. Syst.* **27**, 1429–1444. https://doi.org/10.1109/tnnls.2015.2441137 (2016).

56. Barnett, L., Barrett, A. B. & Seth, A. K. Solved problems for Granger causality in neuroscience: A response to Stokes and Purdon. *NeuroImage* **178**, 744–748. https://doi.org/10.1016/j.neuroimage.2018.05.067 (2018).

57. Bressler, S. L., Kumar, A. & Singer, I. Brain synchronization and multivariate autoregressive (MVAR) modeling in cognitive neurodynamics. *Front. Syst. Neurosci.* **15**, 638269. https://doi.org/10.3389/fnsys.2021.638269 (2022).

58. Manomaisaowapak, P., Nartkulpat, A. & Songsiri, J. Granger causality inference in EEG source connectivity analysis: A state-space approach. *IEEE Trans. Neural Netw. Learn. Syst.* **33**, 3146–3156. https://doi.org/10.1109/tnnls.2021.3096642 (2022).

59. Goshvarpour, A. & Goshvarpour, A. Emotion recognition using a novel Granger causality quantifier and combined electrodes of EEG. *Brain Sci.* **13**, 759. https://doi.org/10.3390/brainsci13050759 (2023).

60. He, F. & Yang, Y. Nonlinear system identification of neural systems from neurophysiological signals. *Neuroscience* **458**, 213–228. https://doi.org/10.1016/j.neuroscience.2020.12.001 (2021).

61. Darvas, F., Ojemann, J. & Sorensen, L. Bi-phase locking—a tool for probing non-linear interaction in the human brain. *NeuroImage* **46**, 123–132. https://doi.org/10.1016/j.neuroimage.2009.01.034 (2009).

62. Sameni, R. & Seraj, E. A robust statistical framework for instantaneous electroencephalogram phase and frequency estimation and analysis. *Physiol. Meas.* **38**, 2141–2163. https://doi.org/10.1088/1361-6579/aa93a1 (2017).

63. Aru, J. *et al.* Untangling cross-frequency coupling in neuroscience. *Curr. Opin. Neurobiol.* **31**, 51–61. https://doi.org/10.1016/j.conb.2014.08.002 (2015).

64. Wang, X., Chen, Y. & Ding, M. Testing for statistical significance in bispectra: A surrogate data approach and application to neuroscience. *IEEE Trans. Biomed. Eng.* **54**, 1974–1982. https://doi.org/10.1109/TBME.2007.895751 (2007).

65. Chella, F., Marzetti, L., Pizzella, V., Zappasodi, F. & Nolte, G. Third order spectral analysis robust to mixing artifacts for mapping cross-frequency interactions in EEG/MEG. *NeuroImage* **91**, 146–161. https://doi.org/10.1016/j.neuroimage.2013.12.064 (2014).

66. Clemson, P., Lancaster, G. & Stefanovska, A. Reconstructing time-dependent dynamics. *Proc. IEEE* **104**, 223–241. https://doi.org/10.1109/JPROC.2015.2491262 (2016).

67. Hadjileontiadis, L. J. Continuous wavelet transform and higher-order spectrum: Combinatory potentialities in breath sound analysis and electroencephalogram-based pain characterization. *Philos. Trans. A Math. Phys. Eng. Sci.* **376**, 20170249. https://doi.org/10.1098/rsta.2017.0249 (2018).

68. Li, X., Li, D., Voss, L. J. & Sleigh, J. W. The comodulation measure of neuronal oscillations with general harmonic wavelet bicoherence and application to sleep analysis. *NeuroImage* **48**, 501–514. https://doi.org/10.1016/j.neuroimage.2009.07.008 (2009).

69. Chua, K. C., Chandran, V., Acharya, U. R. & Lim, C. M. Application of higher order spectra to identify epileptic EEG. *J. Med. Syst.* **35**, 1563–1571. https://doi.org/10.1007/s10916-010-9433-z (2011).

70. Schiecke, K. *et al.* Time-variant, frequency-selective, linear and nonlinear analysis of heart rate variability in children with temporal lobe epilepsy. *IEEE Trans. Biomed. Eng.* **61**, 1798–1808. https://doi.org/10.1109/TBME.2014.2307481 (2014).

71. Hosseini, S. A. A hybrid approach based on higher order spectra for clinical recognition of seizure and epilepsy using brain activity. *Basic Clin. Neurosci.* **8**, 479–492. https://doi.org/10.29252/NIRP.BCN.8.6.479 (2017).

72. Wang, R. *et al.* Multiple feature extraction and classification of electroencephalograph signal for Alzheimers' with spectrum and bispectrum. *Chaos* **25**, 013110. https://doi.org/10.1063/1.4906038 (2015).

73. Nasrolahzadeh, M., Mohammadpoory, Z. & Haddadnia, J. A novel method for early diagnosis of Alzheimer's disease based on higher-order spectral estimation of spontaneous speech signals. *Cogn. Neurodyn.* **10**, 495–503. https://doi.org/10.1007/s11571-016-9406-0 (2016).

74. Maturana-Candelas, A., Gómez, C., Poza, J., Ruiz-Gómez, S. J. & Hornero, R. Inter-band bispectral analysis of EEG background activity to characterize Alzheimer's disease continuum. *Front. Comput. Neurosci.* **14**, 70. https://doi.org/10.3389/fncom.2020.00070 (2020).

75. Lii, K. S. & Helland, K. N. Cross-bispectrum computation and variance estimation. *ACM Trans. Math. Softw.* **7**, 284–294. https://doi.org/10.1145/355958.355961 (1981).

76. Abe, T. *rhosa: Higher-Order Spectral Analysis*. R package version 0.2.0 (2022).

77. Schelter, B., Timmer, J. & Eichler, M. Assessing the strength of directed influences among neural signals using renormalized partial directed coherence. *J. Neurosci. Methods* **179**, 121–30. https://doi.org/10.1016/j.jneumeth.2009.01.006 (2009).

78. Benjamini, Y. & Hochberg, Y. Controlling the false discovery rate: A practical and powerful approach to multiple testing. *J. R. Stat. Soc. Ser. B (Methodol.)* **57**, 289–300. https://doi.org/10.1111/j.2517-6161.1995.tb02031.x (1995).

79. Kwong, K. S., Holland, B. & Cheung, S. H. A modified Benjamini–Hochberg multiple comparisons procedure for controlling the false discovery rate. *J. Stat. Plan. Inference* **104**, 351–362. https://doi.org/10.1016/S0378-3758(01)00252-X (2002).

80. Colquhoun, D. An investigation of the false discovery rate and the misinterpretation of *p*-values. *R. Soc. Open Sci.* **1**, 140216. https://doi.org/10.1098/rsos.140216 (2014).

81. Schwartzman, A. Empirical null and false discovery rate inference for exponential families. *Ann. Appl. Stat.* **2**, 1332–1359. https://doi.org/10.1214/08-AOAS184 (2008).

82. Kim, Y. C. & Powers, E. J. Digital bispectral analysis and its applications to nonlinear wave interactions. *IEEE Trans. Plasma Sci.* **7**, 120–131. https://doi.org/10.1109/TPS.1979.4317207 (1979).

83. Nikias, C. L. & Raghuveer, M. R. Bispectrum estimation: A digital signal processing framework. *Proc. IEEE* **75**, 869–891. https://doi.org/10.1109/PROC.1987.13824 (1987).

84. Sherman, D. L. & Zoltowski, M. D. Matrix-based higher order spectral analysis for three-wave coupling processes. *IEEE Trans. Signal Process.* **42**, 332–348. https://doi.org/10.1109/78.275606 (1994).

85. Randall, R. B. *Frequency Analysis* 3rd edn, 344 (Bruël and Kjær, 1987).

86. Cerna, M. & Harvey, A. F. The fundamentals of FFT-based signal analysis and measurement. Application Note 041, National Instruments Corporation (2000).

87. Welch, P. The use of fast Fourier transform for the estimation of power spectra: A method based on time averaging over short, modified periodograms. *IEEE Trans. Audio Electroacoust.* **15**, 70–73. https://doi.org/10.1109/TAU.1967.1161901 (1967).

88. Dhamala, M., Rangarajan, G. & Ding, M. Estimating Granger causality from Fourier and wavelet transforms of time series data. *Phys. Rev. Lett.* **100**, 018701. https://doi.org/10.1103/PhysRevLett.100.018701 (2008).

89. Pfaff, B. *Analysis of Integrated and Cointegrated Time Series with R* 2nd edn, 188 (Springer, New York, 2008).

90. Schwarz, G. Estimating the dimension of a model. *Ann. Stat.* **6**, 461–464. https://doi.org/10.1214/aos/1176344136 (1978).

91. Ventzislav, I. & Lutz, K. A practitioner's guide to lag order selection For VAR impulse response analysis. *Stud. Nonlinear Dyn. Econ.* **9**, 1–36. https://doi.org/10.2202/1558-3708.1219 (2005).

92. Storey, J. D. The positive false discovery rate: A Bayesian interpretation and the q-value. *Ann. Stat.* **31**, 2013–2035. https://doi.org/10.1214/aos/1074290335 (2003).

93. Storey, J. D., Xiao, W., Leek, J. T., Tompkins, R. G. & Davis, R. W. Significance analysis of time course microarray experiments. *Proc. Natl. Acad. Sci. U. S. A.* **102**, 12837–12842. https://doi.org/10.1073/pnas.0504609102 (2005).

Author contributions

All authors conceived the study; T.A. contributed with new analytic tools and program code for R package; T.A., A.E.P.V. analyzed the results and prepared the figures; all authors contributed to the written version of the paper and revised its final version.

Competing interests

The authors declare no competing interests.

Additional information

Supplementary Information The online version contains supplementary material available at https://doi.org/10.1038/s41598-024-59004-8.

Correspondence and requests for materials should be addressed to A.E.P.V.

Reprints and permissions information is available at www.nature.com/reprints.

Publisher's note Springer Nature remains neutral with regard to jurisdictional claims in published maps and institutional affiliations.